INTERNATIONAL JOURNAL FOR NUMERICAL METHODS IN ENGINEERING
Int. J. Numer. Meth. Engng 2002; **54**:1623–1648 (DOI: 10.1002/nme.489)

A point interpolation meshless method based on radial basis functions

J. G. Wang*,† and G. R. Liu

Centre for Advanced Computations in Engineering Science, Department of Mechanical Engineering, National University of Singapore, 10 Kent Ridge Crescent, Singapore 119260, Singapore

SUMMARY

A point interpolation meshless method is proposed based on combining radial and polynomial basis functions. Involvement of radial basis functions overcomes possible singularity associated with the meshless methods based on only the polynomial basis. This non-singularity is useful in constructing well-performed shape functions. Furthermore, the interpolation function obtained passes through all scattered points in an influence domain and thus shape functions are of delta function property. This makes the implementation of essential boundary conditions much easier than the meshless methods based on the moving least-squares approximation. In addition, the partial derivatives of shape functions are easily obtained, thus improving computational efficiency. Examples on curve/surface fittings and solid mechanics problems show that the accuracy and convergence rate of the present method is high.

KEY WORDS: meshless method; point interpolation; radial basis function; singularity; stress analysis

1. INTRODUCTION

Computer applications have made numerical simulations a daily activity for engineering science. Most numerical simulations are carried out with the help of the finite element method (FEM). However, the essence of the FEM is that a problem domain can be divided into small elements. These elements are not overlapping each other. Any field function is approximated within each element through simple interpolation functions. If the element is heavily distorted, shape functions for this element are of poor quality and thus the numerical results may not be acceptable. One scheme to solve element distortions is to re-mesh the local domain and to develop adaptive techniques. Adaptive techniques have been active in numerical algorithms. Being different from element-based technique, meshless methods approximate field functions within an influence domain instead of an element. The nodes in each influence domain may

*Correspondence to: J. G. Wang, Tropical Marine Science Institute, National University of Singapore, 10 Kent Ridge Crescent, Singapore 119260, Singapore.
†E-mail: tmswjg@nus.edu.sg

Received 2 November 1999
Revised 20 November 2001

be arbitrarily distributed or unstructured. Different influence domains may and must overlap. The element-based disadvantage does not occur any more in the meshless methods.

Meshless methods have been achieved remarkable progress in recent years. Main efforts have been focusing on different approximation methods over a cluster of scattered nodes. For example, diffuse element method (DEM) [1] was the first meshless method to employ moving least-squares approximation (MLS) in constructing their shape functions over scattered nodes instead of an element. The MLS was originally proposed by Lancaster and Salkauskas [2] for surface fitting. Belytschko and his colleagues (see References [3–5]) extended the DEM to more solid foundation within the framework of Galerkin weak form and developed an element-free Galerkin (EFG) method. Smooth particle hydrodynamics method (SPH) [6] is one of the oldest and well-developed meshless methods. It was based on a kernel approximation. Reproducing kernel particle method (RKPM) [7] further extended the SPH method with improved continuity (by correction function) and multiple scales (by window function). Radial basis functions are also attractive in the development of meshless methods. HP-cloud method [8] was based on an improved Shepard method [9] which is widely used in data fitting. A finite point method (FPM) [10] was proposed to construct the basis functions through a local Taylor expansion. The FPM has been applied to the problems in fluid mechanics. Belytschko concluded in his review paper [4] that the MLS approximation was the fundamental for all kinds of above-mentioned meshless methods. Although the meshless methods based on the MLS have been successfully applied in computational mechanics, two major technical issues are still not well solved: (i) Difficulties in the implementation of essential boundary conditions. This is because its shape functions are short of delta function properties. (ii) Complexity in numerical algorithms for computing shape functions and their derivatives. For the first issue, many schemes have been proposed such as Lagrangian [5], penalty [11] and collocation [12]. For the second issue, some useful algorithms have been proposed such as analytical integration [7], recursive method [13] and parallel computing [14].

A point interpolation method (PIM) was proposed to address above two issues [15, 16]. The PIM seems attractive in several ways. First, its approximation function passes through each node in an influence domain and thus its shape functions are of delta function properties. Second, its shape functions are simple compared to MLS. Third, its shape functions and derivatives are easily developed only if basis functions are selected. The original PIM [15] employed only polynomials as its basis functions and thus special techniques were required to guarantee a successful computation of shape functions for an arbitrarily chosen set of scattered points [15, 17].

This paper proposes a point interpolation meshless method based on radial basis functions for the solution of partial differential equations. This forms a radial PIM. Particularly, Gaussian and multiquadric radial basis functions [18] are applied in the radial PIM. Historically, the approximation techniques through radial basis functions were developed for curve/surface fittings. Its application in partial differential equations was encouraged by the pioneer work done by Kansa [19]. Kansa's algorithm was similar to finite difference method (FDM), but node distribution was completely unstructured. Recently, collocation methods were developed, e.g. in References [20–22]. Our proposed method combines the Galerkin weak form and radial basis functions to form a radial PIM. This method is different from other methods in following three aspects. First, the interpolation is carried out within an influence domain instead of global domain even the radial basis functions selected are global type instead of compactly supported type [21, 23]. The system matrix is sparse and banded and thus this

method is more suitable for large-scale problems. This local interpolation is a little different from the methods developed for curve/surface fittings where the condition number is a big problem for tens of thousands of nodes [24–26]. Second, the node distribution within an influence domain is completely unstructured. This is different from the PIM based on only polynomial basis functions where the singularity may occur sometimes. Third, as discussed in our paper [27], the accuracy of the radial PIM depends not only on the accuracy of function approximation but also on the weak form [28].

This paper is organized as follows: point interpolation approximation is described in Section 2 for combination of general radial and polynomial basis functions. Their properties of shape functions are discussed and the particular forms of Gaussian and multiquadric basis functions are suggested in Section 3. Curve and surface fittings as examples are studied in Section 4 to investigate the capacity and accuracy of proposed radial PIM approximations under different shape parameters. A Galerkin weak form and its numerical algorithm are studied for solid mechanics problems in Section 5. The accuracy and convergence ratio are studied through patch test and some examples in Section 6. Finally, Section 7 draws the conclusion.

2. POINT INTERPOLATION BASED ON RADIAL BASIS FUNCTION

Consider an approximation function $u(\mathbf{x})$ in an influence domain that has a set of arbitrarily distributed nodes $P_i(\mathbf{x}_i)$ $(i=1,2,\ldots,n)$. n is the number of nodes in the influence domain of $\mathbf{x}$. Nodal function value is assumed to be u_i at the node $\mathbf{x}_i$. Radial PIM constructs the approximation function $u(\mathbf{x})$ to pass through all these node points using radial basis function $B_i(\mathbf{x})$ and polynomial basis function $p_j(\mathbf{x})$ [24]

$$u(\mathbf{x})=\sum_{i=1}^{n} B_i(\mathbf{x})a_i + \sum_{j=1}^{m} P_j(\mathbf{x})b_j = \mathbf{B}^{\mathrm{T}}(\mathbf{x})\mathbf{a} + \mathbf{P}^{\mathrm{T}}(\mathbf{x})\mathbf{b} \tag{1}$$

where a_i is the coefficient for $B_i(\mathbf{x})$ and b_j the coefficient for $p_i(\mathbf{x})$ (usually, $m<n$). The vectors are defined as

$$\begin{aligned} \mathbf{a}^{\mathrm{T}} &= [a_1, a_2, a_3, \ldots, a_n] \\ \mathbf{b}^{\mathrm{T}} &= [b_1, b_2, \ldots, b_m] \\ \mathbf{B}^{\mathrm{T}}(\mathbf{x}) &= [B_1(\mathbf{x}), B_2(\mathbf{x}), B_3(\mathbf{x}), \ldots, B_n(\mathbf{x})] \\ \mathbf{P}^{\mathrm{T}}(\mathbf{x}) &= [p_1(\mathbf{x}), p_2(\mathbf{x}), \ldots, p_m(\mathbf{x})] \end{aligned} \tag{2}$$

Basis functions are usually the functions of co-ordinates $\mathbf{x}^{\mathrm{T}}=[x, y]$ for two-dimensional problems. A radial basis function has the following general form:

$$B_i(\mathbf{x})=B_i(r_i)=B_i(x, y) \tag{3}$$

where r_i is a distance between interpolating point (x, y) and the node (x_i, y_i). This distance in the Euclidean two-dimensional space is expressed as

$$r_i=[(x-x_i)^2+(y-y_i)^2]^{1/2} \tag{4}$$

A polynomial basis function has the following monomial terms as:

$$\mathbf{P}^{\mathrm{T}}(\mathbf{x})=[1,\ x,\ y,\ x^2,xy,y^2,\ldots] \tag{5}$$

The coefficients a_i and b_j in Equation (1) are determined by enforcing the interpolation pass through all n scattered nodal points within the influence domain. The interpolation at the kth point has

$$u_k=u(x_k,y_k)=\sum_{i=1}^{n}a_iB_i(x_k,y_k)+\sum_{j=1}^{m}b_jP_j(x_k,y_k),\quad k=1,2,\ldots,n \tag{6}$$

The polynomial term is an extra-requirement that guarantees unique approximation [28]. Following constraints are usually imposed:

$$\sum_{i=1}^{n}P_j(x_i,y_i)a_i=0,\quad j=1,2,\ldots,m \tag{7}$$

It is expressed in matrix form as follows:

$$\begin{bmatrix}\mathbf{B}_0 & \mathbf{P}_0\\ \mathbf{P}_0^{\mathrm{T}} & \mathbf{0}\end{bmatrix}\begin{Bmatrix}\mathbf{a}\\ \mathbf{b}\end{Bmatrix}=\begin{Bmatrix}\mathbf{u}^e\\ \mathbf{0}\end{Bmatrix}\quad\text{or}\quad\mathbf{G}\begin{Bmatrix}\mathbf{a}\\ \mathbf{b}\end{Bmatrix}=\begin{Bmatrix}\mathbf{u}^e\\ \mathbf{0}\end{Bmatrix} \tag{8}$$

where the vector for function values is defined as

$$\mathbf{u}^e=[u_1,u_2,u_3,\ldots,u_n]^{\mathrm{T}} \tag{9}$$

The coefficient matrix $\mathbf{B}_0$ on unknowns $\mathbf{a}$ is

$$\mathbf{B}_0=\begin{bmatrix}B_1(x_1,y_1) & B_2(x_1,y_1) & \cdots & B_n(x_1,y_1)\\ B_1(x_2,y_2) & B_2(x_2,y_2) & \cdots & B_n(x_2,y_2)\\ \vdots & \vdots & \vdots & \vdots\\ B_1(x_n,y_n) & B_2(x_n,y_n) & \cdots & B_n(x_n,y_n)\end{bmatrix}_{n\times n} \tag{10}$$

The coefficient matrix $\mathbf{P}_0$ on unknowns $\mathbf{b}$ is

$$\mathbf{P}_0=\begin{bmatrix}P_1(x_1,y_1) & P_2(x_1,y_1) & \cdots & P_m(x_1,y_1)\\ P_1(x_2,y_2) & P_2(x_2,y_2) & \cdots & P_m(x_2,y_2)\\ \vdots & \vdots & \vdots & \vdots\\ P_1(x_n,y_n) & P_2(x_n,y_n) & \cdots & P_m(x_n,y_n)\end{bmatrix}_{n\times m} \tag{11}$$

Because the distance is directionless, there is $B_k(x_i,y_i)=B_i(x_k,y_k)$, which means that the matrix $\mathbf{B}_0$ is symmetric. Unique solution is obtained if the inverse of matrix $\mathbf{B}_0$ exists,

$$\begin{Bmatrix}\mathbf{a}\\ \mathbf{b}\end{Bmatrix}=\mathbf{G}^{-1}\begin{Bmatrix}\mathbf{u}^e\\ \mathbf{0}\end{Bmatrix} \tag{12}$$

The interpolation is finally expressed as

$$u(\mathbf{x})=[\mathbf{B}^{\mathrm{T}}(\mathbf{x}) \quad \mathbf{P}^{\mathrm{T}}(\mathbf{x})]\mathbf{G}^{-1}\begin{Bmatrix}\mathbf{u}^e\\ \mathbf{0}\end{Bmatrix}=\boldsymbol{\varphi}(\mathbf{x})\mathbf{u}^e \tag{13}$$

where the matrix of shape functions $\boldsymbol{\varphi}(\mathbf{x})$ is defined by

$$\boldsymbol{\varphi}(\mathbf{x})=[\phi_1(\mathbf{x}),\phi_2(\mathbf{x}),\ldots,\phi_i(\mathbf{x}),\ldots,\phi_n(\mathbf{x})] \tag{14}$$

in which

$$\phi_k(\mathbf{x})=\sum_{i=1}^{n} B_i(\mathbf{x})\bar{G}_{i,k}+\sum_{j=1}^{m} P_j(\mathbf{x})\bar{G}_{n+j,k} \tag{15}$$

where $\bar{G}_{i,k}$ is the (i,k) element of matrix $\mathbf{G}^{-1}$. After radial basis functions are determined, shape functions depend only upon the position of scattered nodes. Once the inverse of matrix $\mathbf{G}$ is obtained, the derivatives of shape functions are easily obtained as

$$\begin{aligned}\frac{\partial\phi_k}{\partial x} &= \sum_{i=1}^{n}\frac{\partial B_i}{\partial x}\bar{G}_{i,k}+\sum_{j=1}^{m}\frac{\partial P_j}{\partial x}\bar{G}_{n+j,k}\\ \frac{\partial\phi_k}{\partial y} &= \sum_{i=1}^{n}\frac{\partial B_i}{\partial y}\bar{G}_{i,k}+\sum_{j=1}^{m}\frac{\partial P_j}{\partial y}\bar{G}_{n+j,k}\end{aligned} \tag{16}$$

3. PROPERTIES OF SHAPE FUNCTIONS

The shape functions $\phi_i(\mathbf{x})$ depend uniquely on the distribution of scattered nodes after all basis functions are determined. Generally, the shape functions have following properties regardless of particular forms of radial basis functions:

(1) Shape functions are linearly independent in the influence domain. This is because basis functions are of linear independence within the influence domain. If $\mathbf{B}_0^{-1}$ and its extension $\mathbf{G}^{-1}$ exist for arbitrary scattered data points, the shape functions and the basis functions are equivalent in function space. For the Gaussian radial basis function, Powell [24] has proved that the inverse always exists regardless of its shape parameters. This is the major advantage of radial basis over polynomial basis.

(2) Shape functions are of delta function properties, that is

$$\phi_i(\mathbf{x}=\mathbf{x}_j)=\begin{cases}1, & i=j,\ \ j=1,2,\ldots,n\\ 0, & i\neq j,\ \ i,j=1,2,\ldots,n\end{cases} \tag{17}$$

Because u_i is independent of shape function $\phi_i(\mathbf{x})$, let $u^e=\{0,0,\ldots,u_i,\ldots,0\}^{\mathrm{T}}$. That is, all nodes have zero values except the ith node. Equation (13) holds true even for such a case, thus producing Equation (17). Figure 1 shows a typical shape function for Gaussian and multiquadric basis functions in one- and two-dimensional space. The shape functions are decreasing with radial distance for the selected shape parameters.

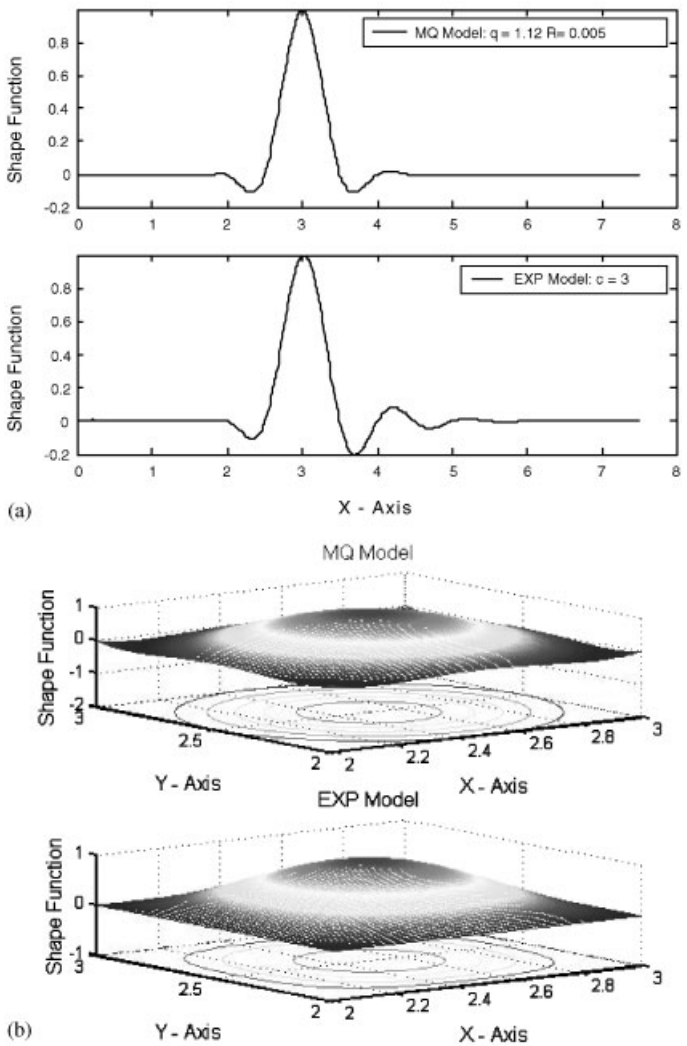

Figure 1. (a) Shape function for one-dimensional domain; and (b) shape function for two-dimensional domain.

(3) $\phi_i(\mathbf{x})$ is of unity partition as

$$\sum_{i=1}^{n} \phi_i(\mathbf{x}) = 1 \tag{18}$$

It should be noted that there does not require $0 \leqslant \phi_i(\mathbf{x}) \leqslant 1$.

(4) $\phi_i(\mathbf{x})$ is of reproducing properties as

$$\sum_{i=1}^{n} \phi_i(\mathbf{x}) x_i = \mathbf{x} \tag{19}$$

Equations (18) and (19) always hold if basis functions include at least the first-order polynomial. As the polynomial basis $[1, x, y](m=3)$ is included in Equation (1), the shape functions so developed satisfy Equations (18) and (19).

(5) $\phi_i(\mathbf{x})$ has simple derivatives.

(6) Local compact support.

Because the point interpolation is carried out in an influence domain and each influence domain is localized. That implies that a weight function with one in the domain and zero outside the domain is imposed during interpolation. The system matrix obtained is sparse and banded. This property distinguishes the radial PIM from global methods. It should be noted that this interpolation is also different from Wendland's method [21, 23] where a compactly supported basis is constructed.

Two particular forms of radial basis functions $B_i(x, y)$ are introduced hereafter although radial basis functions may have other forms such as compactly supported forms [21, 23]. A classical form is multiquadric basis (called MQ) proposed by Hardy [18]. This form has been widely used in surface fitting and solution of partial differential equations [19–28]. We extend the original form of multiquadric to following general form (called MQ, too) in this paper

$$B_i(x, y)=(r_i^2 + R^2)^q \tag{20}$$

where q and R are two shape parameters. When $q=0.5$, Equation (20) becomes the original MQ. When $q=-0.5$, it reduces to the reciprocal multiquadric (RMQ). Its partial derivatives are obtained as follows:

$$\begin{aligned} \frac{\partial B_i}{\partial x} &= 2q(r_i^2 + R^2)^{q-1}(x - x_i) \\ \frac{\partial B_i}{\partial y} &= 2q(r_i^2 + R^2)^{q-1}(y - y_i) \end{aligned} \tag{21}$$

Gaussian form is well known [24]. Although it was always used as a global function such as Reference [22], Gaussian form will be used as radial basis function in an influence domain in this paper

$$B_i(x, y)= \exp(-cr_i^2) \tag{22}$$

where c is a shape parameter. Its partial derivatives are again obtained as follows:

$$\begin{aligned} \frac{\partial B_i}{\partial x} &= -2cB_i(x, y)(x - x_i) \\ \frac{\partial B_i}{\partial y} &= -2cB_i(x, y)(y - y_i) \end{aligned} \tag{23}$$

The present method using Gaussian basis function is called EXP method herein.

4. ANALYSIS OF SHAPE PARAMETERS THROUGH CURVE AND SURFACE FITTING

Curve and surface fitting capability of above two types of radial basis functions is evaluated through one- and two-dimensional functions. General evaluations were given by Franke [29] for various interpolations. Being different from his evaluation, analysis of shape parameters is emphasized in this paper. Because linear functions in one- and two-dimensional spaces can be reproduced exactly when $m=3$, the test functions do not include linear functions any more. Furthermore, because radial basis functions are focused on, polynomial basis is omitted in this section (i.e. $m=0$). This omission does not affect the evaluation of shape parameters [27]. It is noted that the evaluation data sets are generated by the given functions with regular and irregular node distributions.

4.1. Procedure for curve fitting

Following three functions are tested in the domain $[0,7]$. Node distribution as shown in Figure 2(a) is used for all curve fittings:

$$f_1=\sin(x), \quad f_2=\sin^2(x)+(0.5x-1)\cos(x), \quad f_3=\frac{x^2}{8+x^5} \tag{24}$$

The first function is typically oscillatory with x. The second is a mixture of polynomial and harmonic series. The last is a fractional function that approaches to zero when x approaches to infinity. All of them are different from radial and polynomial basis functions. Their derivatives are as follows:

$$\begin{aligned} f_1' &= \cos(x) \\ f_2' &= 2\sin(x)\cos(x)-(0.5x-1)\sin(x)+0.5\cos(x) \\ f_3' &= \frac{16x-3x^6}{(8+x^5)^2} \end{aligned} \tag{25}$$

Following procedure is adopted for curve fittings:

(a) Give a set of (x_i, f_i) $(i=1,2,\ldots,n)$ for each function to set up a set of nodes.
(b) Determine the matrix $\mathbf{B}_0$ and $\mathbf{P}_0$ in Equations (10) and (11) from this set of nodes.
(c) Solve Equation (8) to get the coefficients **a** and **b**
(d) Choose a set of interpolation points x_j $(j=1,2,\ldots,k)$ arbitrarily in the domain. It is better that this set includes the node x_i as a subset.
(e) Calculate interpolation values through interpolation function of Equation (13) and its derivatives with respect to x through Equation (16).
(f) Calculate real function and its derivatives at the same interpolation point x_j $(j=1,2,\ldots,k)$.
(g) Plot interpolation and real functions for comparison.

4.2. Error analysis and shape parameters

Fitting capability and shape parameters are investigated for the two basis functions, MQ and EXP. Figures 2–4 give the comparisons between fitting curve and real function and their derivatives through MQ interpolation. Figure 2 gives the sine function and its derivatives.

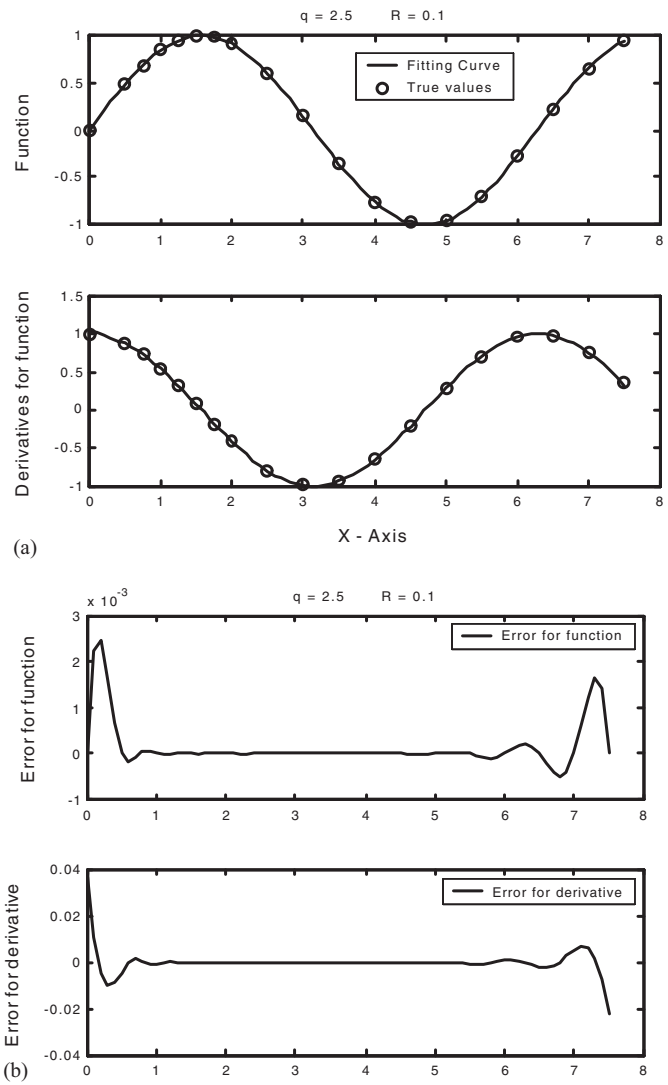

Figure 2. MQ interpolation for $f_1 = \sin(x)$: (a) fitting for function and derivatives; and (b) error analysis for function f_1.

Figure 3 has the similar results. Both function and derivative are matching very well. For the fractional function, fitting results are less accurate as shown in Figure 4. EXP interpolation gives similar results and a typical result is shown in Figure 5. Based on our computations, following remarks can be made:

For MQ interpolation:

(a) When q is larger than zero and approaches to zero, fitting accuracy is not good. The smaller the shape parameter q, the more inaccurate fitting curves and their derivatives

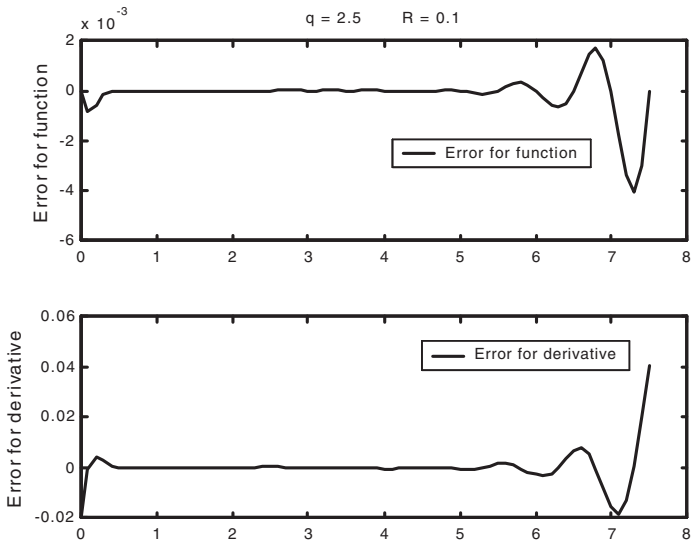

Figure 3. Error analysis of MQ interpolation for $f_2 = \sin^2(x) + (0.5x - 1)\cos(x)$.

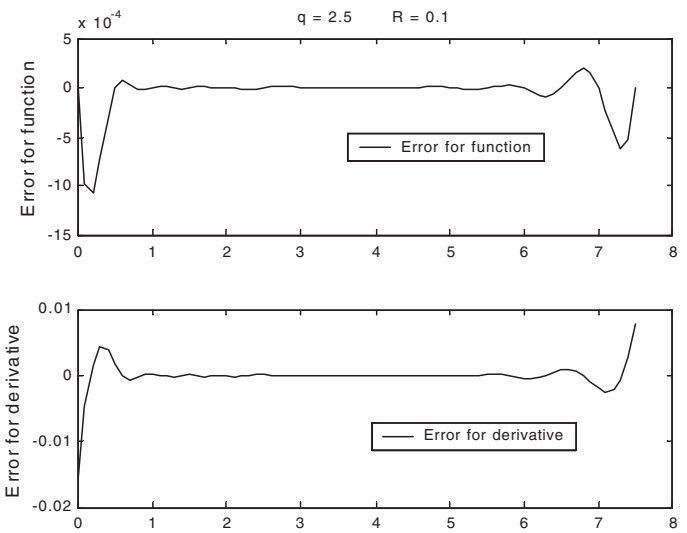

Figure 4. Error analysis of MQ interpolation for $f_3 = \dfrac{x^2}{8 + x^5}$.

are, although condition number of matrix $\mathbf{B}_0$ is small as shown in Figure 6(a). Smaller shape parameter R has smaller condition number. The matrices $\mathbf{G}$ and $\mathbf{B}_0$ have similar condition numbers for MQ and EXP basis functions.

(b) When $0 < q < 1$, function fitting is smooth, while derivatives are still oscillatory. When q is integer, the matrix $\mathbf{B}_0$ is ill-conditioned.

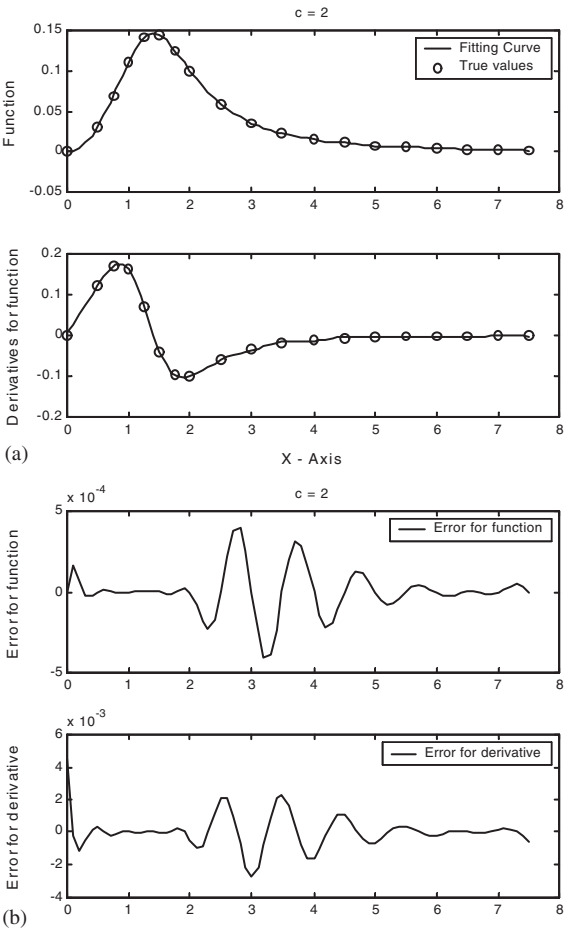

Figure 5. EXP interpolation for $f_3 = \dfrac{x^2}{8+x^5}$: (a) curve fitting of EXP interpolation for f_3; and (b) error analysis for function f_3.

(c) When $1 < q < 3.5$ function and its derivatives are better and better with increasing of q. They have sufficient smoothness although the condition number is bigger.
(d) When $3.5 < q < 10$ fitting results get worse if bigger q is taken. When $q = 10$, the fitting results become unacceptable.
(e) Functions and derivatives have much bigger error near the domain edge.

For EXP interpolation: Shape parameter c will affect the properties of shape functions. The question is what is the acceptable range of c? The acceptable range may vary slightly from function to function. Our computations show that shape parameter suitable for f_3 function is also suitable for other two. Based on computations, following remarks can be drawn:

(a) Shape parameter c has vital effect on condition number as shown in Figure 6(b). When c is too small (say 0.001), the condition number is too big to be suitable for numerical

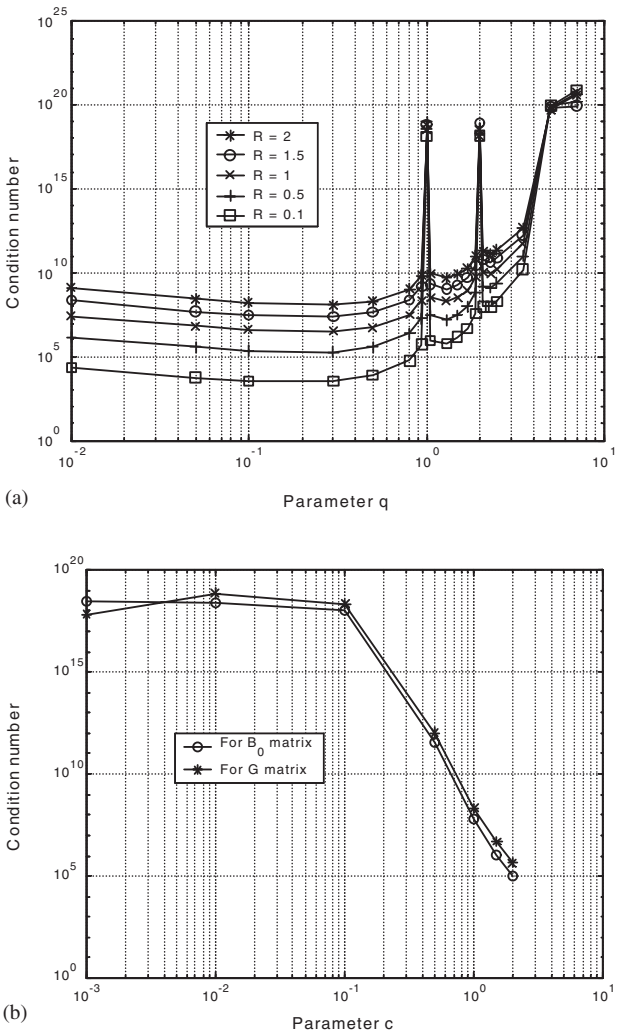

Figure 6. Effect of shape parameters on condition number for two radial basis functions: (a) effect of shape parameters for MQ basis; and (b) effect of shape parameter for EXP basis.

analysis. In this case, fitting function is oscillatory but its derivatives are smooth as shown in Figure 7. Although the inverse is available at this time, the interpolation error is too big to be unacceptable. Therefore, the acceptable range should be larger than some value such as 0.001.

(b) For all shape parameters tested, errors are much bigger at the domain edge. The error dissipates to central points with smaller shape parameter.

(c) Compared to the MQ interpolation, smaller shape parameter c has smooth derivatives, while the condition number of $\mathbf{B}_0$ approaches to infinity as shown in Figure 6(b). MQ interpolation has stable condition number when its shape parameter q is less than 1.0.

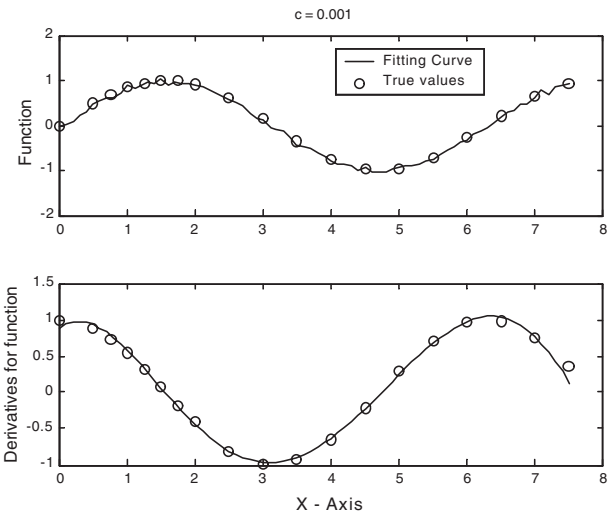

Figure 7. Non-smooth function and smooth derivative by EXP basis functions.

4.3. *Error analysis for surface fitting*

Following two functions are tested in the domain $[2,3]\times[2,3]$:

$$f_4 = \sin(x)\cos(y), \quad f_5 = x^2 y^3 \tag{26}$$

Two patterns of nine (9) data points, regular and irregular distributions in (x, y) co-ordinates, are tested. The same procedure as one-dimensional case is applied. A typical comparison of error between true and interpolated surfaces is given in Figure 8 for MQ and EXP basis. Following understandings are drawn from this comparison:

(a) True and interpolated surfaces are identical at node points. They have a little difference for amid points. The difference depends on shape parameters and true functions. Shape parameters of q and R for MQ and c for EXP are slightly different for one- and two-dimensional problems.
(b) EXP interpolation is a little superior to MQ for the two tested functions because MQ performs less accurately for the tested shape parameters, although theoretical studies have proved that MQ and EXP have the same convergence rate [30, 31]. Shape parameters are important to improve the accuracy of both MQ and EXP interpolations [27]. MQ has two parameters to adapt the accuracy requirement while EXP has only one.
(c) Shape functions decrease gradually when $c>0$ and $q<0$. The non-zero domain is dependent of shape parameters. The smaller the c is, the bigger the non-zero domain. MQ has different properties. The bigger the q, the bigger the non-zero domain is.

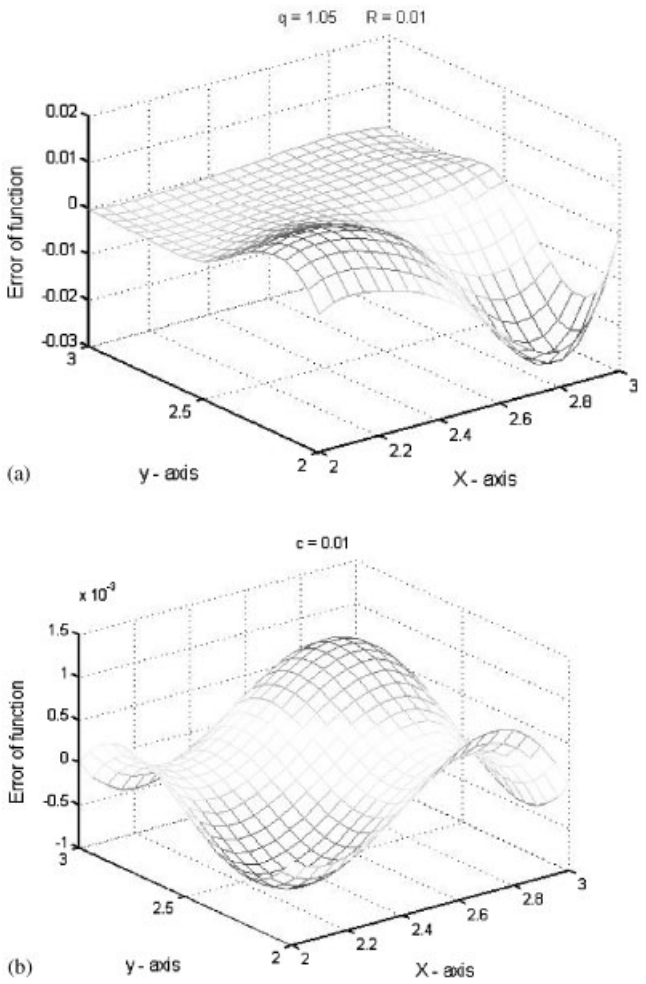

Figure 8. Interpolation accuracy for radial basis (2D cases): (a) error distribution for MQ basis; and (b) error distribution for EXP basis.

5. VARIATIONAL FORM OF PLANE PROBLEM

A two-dimensional problem of solid mechanics will be studied here. The problem can be described by equilibrium, geometrical and constitutive equations in the problem domain Ω bounded by Γ ($\Gamma = \Gamma_t + \Gamma_u$). The equilibrium equation is expressed as

$$\nabla \boldsymbol{\sigma} + \mathbf{F} = 0 \quad \text{in } \Omega \tag{27}$$

where $\boldsymbol{\sigma}$ is the stress tensor and $\mathbf{F}$ the body force vector. Geometrical equation describes the relationship of strain and displacement field $\mathbf{u}$ and constitutive equation links strain and stress.

Boundary conditions are given as follows:

$$\begin{aligned} \boldsymbol{\sigma}\cdot\mathbf{n} &= \bar{\mathbf{t}} \quad \text{on the natural boundary } \Gamma_t \\ \mathbf{u} &= \bar{\mathbf{u}} \quad \text{on the essential boundary } \Gamma_u \end{aligned} \tag{28}$$

in which the superposed bar denotes prescribed boundary values and $\mathbf{n}$ is the unit outward normal to the domain. The weak form for all above equations is expressed as

$$\int_\Omega \delta(\nabla_s \mathbf{u}^{\mathrm{T}})\cdot\boldsymbol{\sigma}\,\mathrm{d}\Omega - \int_\Omega \delta\mathbf{u}^{\mathrm{T}}\cdot\mathbf{F}\,\mathrm{d}\Omega - \int_{\Gamma_t}\delta\mathbf{u}^{\mathrm{T}}\cdot\bar{\mathbf{t}}\,\mathrm{d}\Gamma = 0 \tag{29}$$

Discretization of Equation (29) with Equation (13) yields

$$\mathbf{K}\mathbf{u} = \mathbf{f} \tag{30}$$

where

$$\mathbf{K}_{ij} = \int_\Omega B_i^{\mathrm{T}} D B_j\,\mathrm{d}\Omega, \quad f_i = \int_{\Gamma_t}\phi_i\bar{\mathbf{t}}\,\mathrm{d}\Gamma + \int_\Omega \phi_i\mathbf{F}\,\mathrm{d}\Omega \tag{31}$$

$$B_i = \begin{bmatrix} \phi_{i,x} & 0 \\ 0 & \phi_{i,y} \\ \phi_{i,y} & \phi_{i,x} \end{bmatrix} \tag{32}$$

For linear elasticity, the material matrix $\mathbf{D}$ is expressed as

$$\mathbf{D} = \frac{E}{1-\nu^2}\begin{bmatrix} 1 & \nu & 0 \\ \nu & 1 & 0 \\ 0 & 0 & (1-\nu)/2 \end{bmatrix} \quad \text{for plane stress} \tag{33}$$

A background mesh is necessary to obtain the numerical integrations of Equation (31). This mesh is independent of nodes for interpolations, while FEM uses the same nodes for both interpolation and numerical integration. Gauss quadrature is used for this numerical integration in this paper. Triangular and quadrilateral meshes are compared and their integration accuracy is acceptable.

Following flowchart is used to assemble the stiffness matrix and load vector:

1. Loop over background mesh of domain to determine all Gauss points including its location and weight.
2. Remove the background mesh.
3. Loop over Gauss points
    a. determine influence domain for specified Gauss point and select neighbouring nodes based on a pre-defined criterion;
    b. compute shape function and its derivatives for each Gauss point;
    c. evaluate stiffness and load at each Gauss point;
    d. assemble the contribution of each Gauss point to form system equation.

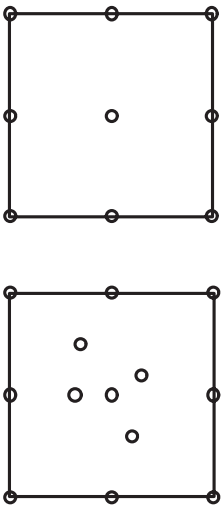

Figure 9. Pattern of nodes for patch test.

4. Introduce essential and loading boundaries (this can be done in influence domain level for radial PIM).
5. Solve the system equation to obtain nodal displacements.
6. Evaluate strain and stress at each Gauss point.

6. NUMERICAL EXAMPLES

6.1. Patch test

Node distributions are shown in Figure 9. A 2×2 rectangular background mesh is used for numerical integration and each mesh uses 3×3 Gauss points. Two types of essential boundaries are given: rigid displacement around the domain and linear displacement assigned along boundary. The radial PIM passes the patch test exactly when $m = 3$ regardless of MQ and EXP basis functions. That is, for the rigid displacement case, displacements within domain are the same as boundary. Stress and strain are all zeros. For the linear displacement case, linear displacement distribution is reproduced and stress is constant within domain. However, when polynomial term is not included ($m = 0$), the patch test does not easily pass. Different radial basis functions have different accuracies. As an example, the linear displacement case is calculated and a typical distribution of displacement at internal nodes is given in Table I when $E = 1$ and $v = 0.3$

6.2. Cantilever beam

6.2.1. Closed-form solution. A cantilever beam problem in Figure 10 is studied here. Consider a beam of length L and height D subjected to traction at the free end. The beam has a unit thickness and hence a plane stress problem is considered. The closed-form solution [32] is

Table I. Patch test results for linear displacement case.

Internal node	Co-ordinates	EXP ($c=0.003$)	MQ ($q=1.03, R=1.0$)
9	(1.0, 1.0)	(0.939, 1.043)	(1.029, 0.9732)
10	(0.65, 1.0)	(0.6548, 1.016)	(0.6496, 1.013)
11	(0.70, 1.5)	(0.817, 1.445)	(0.8607, 1.419)
12	(1.3, 1.2)	(1.246, 1.20)	(1.298, 1.189)
13	(1.2, 0.6)	(1.17, 0.6269)	(1.170, 0.5678)

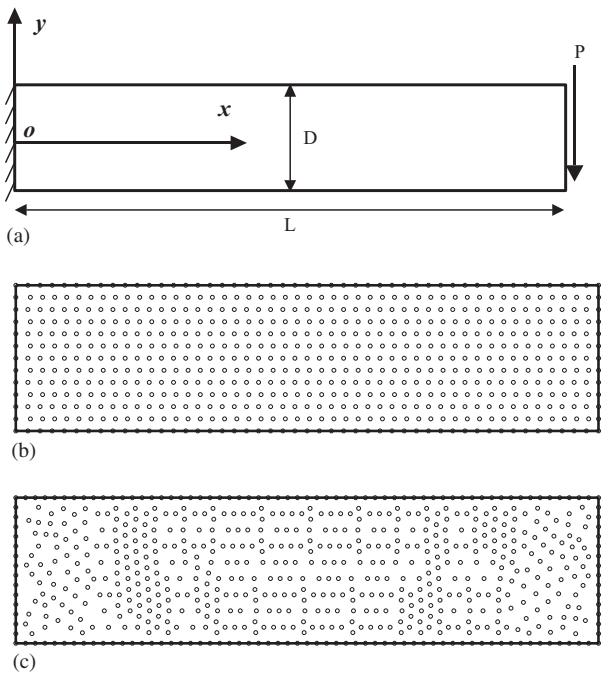

Figure 10. Cantilever beam problem and its meshless models.

available for parabolic traction of force P:

$$u_x = \frac{Py}{6EI}\left[(6L-3x)x+(2+v)\left(y^2-\frac{D^2}{4}\right)\right]$$
$$u_y = -\frac{P}{6EI}\left[3vy^2(L-x)+(4+5v)\frac{D^2x}{4}+(3L-x)x^2\right] \tag{34}$$

where the moment of inertia I of the beam is given $I=D^3/12$.

The stresses corresponding to above displacements are

$$\sigma_x(x,y)=\frac{P(L-x)y}{I}, \quad \sigma_{xy}(x,y)=-\frac{P}{2I}\left[\frac{D^2}{4}-y^2\right], \quad \sigma_y=0 \tag{35}$$

Table II. Error analysis of maximum deflection for different shape parameters.*

EXP method			MQ method ($R=1.42$)		
c	$u_{y\max}$ ($\times 10^{-3}$)	Relative error (%)	q	$u_{y\max}$ ($\times 10^{-3}$)	Relative error (%)
0.001	0.298	−96.7	1.15	7.612	−14.5
0.002	8.59	−3.4	1.10	8.284	−6.9
0.003	8.9	0	1.05	8.767	−1.5
0.005	8.913	0.15	1.03	8.875	−0.28
0.01	8.9	0	0.8	6.816	−23.4
0.03	8.739	−1.8	0.5	4.716	−47.0
0.05	7.901	−11.2	0.2	6.757	−24.1
0.08	5.156	−42.1			
0.1	3.39	−62.0			

*Closed-form solution is $u_{y\max}=8.9\times 10^{-3}$.

The beam parameters are taken as $E=3.0\times 10^7$ kPa, $v=0.3$, $D=12$ m, $L=48$ m and $P=1000$ kN in computation.

6.2.2. Effect of irregular node distribution. Two typical node distributions are shown in Figure 10(b) and 10(c). Regular distribution has 637 nodes while irregular one has 644 nodes. The average node density is almost the same. Background mesh is 576 four-node cells for Figure 10(b) and 1136 three-node cells for Figure 10(c). Shape parameters are $c=0.003$ for EXP and $q=1.03$ and $R=\sqrt{C_I/RP}$ for MQ. Where C_I is a scaling factor of influence domain [3] and takes $C_I=2.0$ and $RP=1.0$. Square influence domain is used for node selection. In our computation, average nodes per Gauss point are 15.16 for regular nodes and 15.7 for irregular nodes. Figure 11 is the sectional distribution of shear stress along $x=24$. Closed-form solution is also plotted for comparison. Both EXP and MQ methods result in excellent agreement regardless of node distributions. Being different from the PIM with polynomial basis [15], radial PIM is not sensitive to node distributions. EXP method has better results than MQ method in this case. The shape parameter R has also effect on numerical results. Reference [27] carries out detailed studies on how shape parameters affect its accuracy.

6.2.3. Effect of shape parameters. Regular node distribution (637), as shown in Figure 10(b), is used to study the effect of shape parameters. The radius of influence domain is fixed as

$$d_{\max}=C_I\times h \tag{36}$$

in which $C_I=2.0$, where h is the maximum distance among neighbouring nodes in the influence domain. Square influence domain is used to select nodes. Such a parameter can select 9–16 nodes for each Gauss point. Basis functions do not include polynomial ($m=0$). Figure 12 shows the effects of shape parameters on the maximum deflection for EXP and MQ. Because R is artificially fixed to 1.42 in MQ method, the q is the only shape parameter. Table II gives the maximum deflections with shape parameters. The results are not sensitive to the shape parameter of EXP radial basis when $c=0.002$–0.03, while MQ method is a little sensitive to the q. When $q=0.5$, which is the original multiquadric [18], the relative error is not acceptable. The minimum error is achieved when $q=1.03$. Of course, the shape

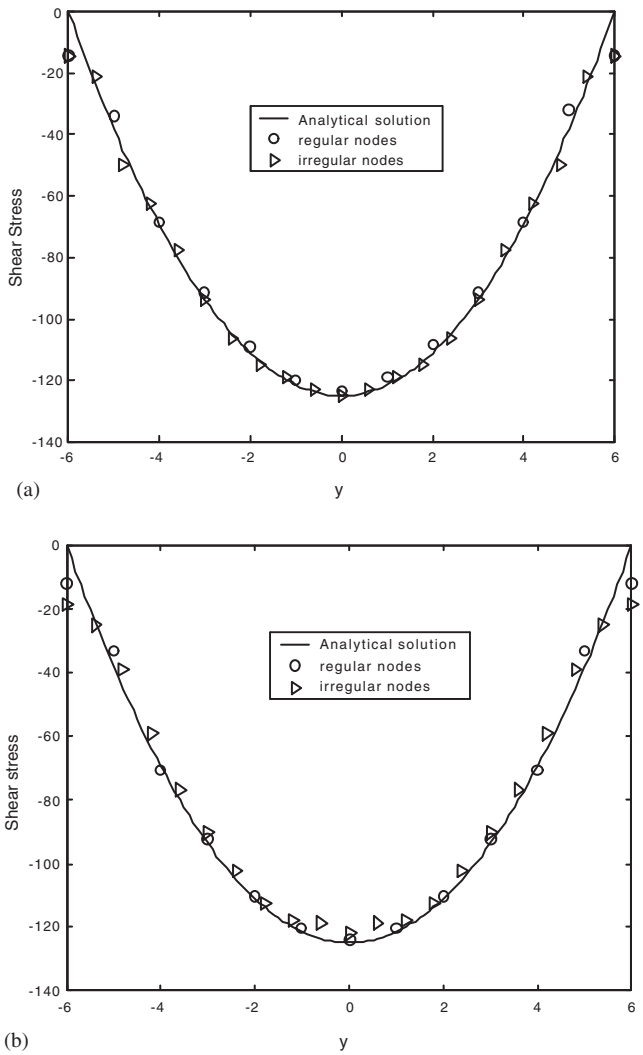

Figure 11. Irregularity effect on shear stress distribution for $x=24$ section: (a) effect of regular and irregular nodes for EXP method; and (b) effect of regular and irregular nodes for MQ method.

parameter R will affect the approximation accuracy of the radial PIM as discussed by many researchers [19, 22, 28].

6.2.4. Convergence rate. An energy norm per unit area is defined as an error indicator, as this indicator comprehensively reflects the accuracy of strain and stress. It is expected that the relationship of indicator with h can express the convergence rate:

$$e_e = \frac{1}{2LD} \int_{\Omega} (\varepsilon^{\mathrm{PIM}} - \varepsilon^{\mathrm{Exact}})^{\mathrm{T}} : (\sigma^{\mathrm{PIM}} - \sigma^{\mathrm{Exact}})\, \mathrm{d}\Omega \tag{37}$$

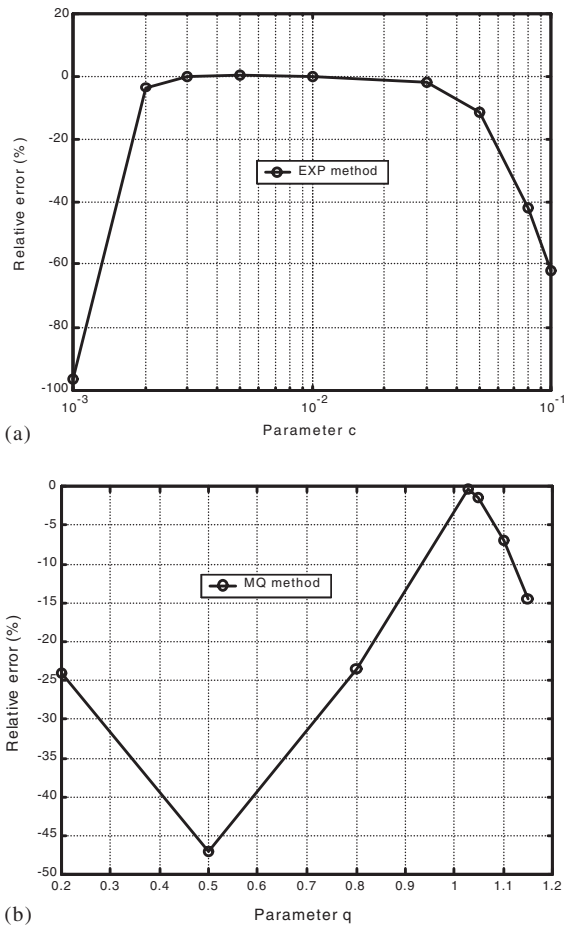

Figure 12. Effect of shape parameters on relative error of maximum deflection: (a) relative error for EXP radial basis functions; and (b) relative error for MQ radial basis functions.

The h is equivalent to the average node distance which is comparable to the element size of FEM method. Regular node distributions (175, 495, 637, 795 and 2425 nodes) are used. Influence domain is determined by Equation (36). Shape parameters are taken as $q=1.03$ for MQ method and $c=0.003$ for EXP method. Figure 13 compares the convergence rates of EXP, MQ and the PIM with polynomial basis. The convergence rates for radial PIM are slightly lower than the PIM with polynomial basis. Generally, the convergence rates are fair good for both radial basis functions.

6.3. Hole in an infinite plate

6.3.1. Closed-form solution. Consider now a plate with a central circular hole subjected to a unidirectional tensile load of 1.0 in the x direction. Only quarter of the plate is simulated due to symmetry. The node distribution (209 nodes) is shown in Figure 14. This is a typical plane stress problem. The material properties are $E=3.0\times10^3$ kPa and $v=0.3$. Symmetry conditions

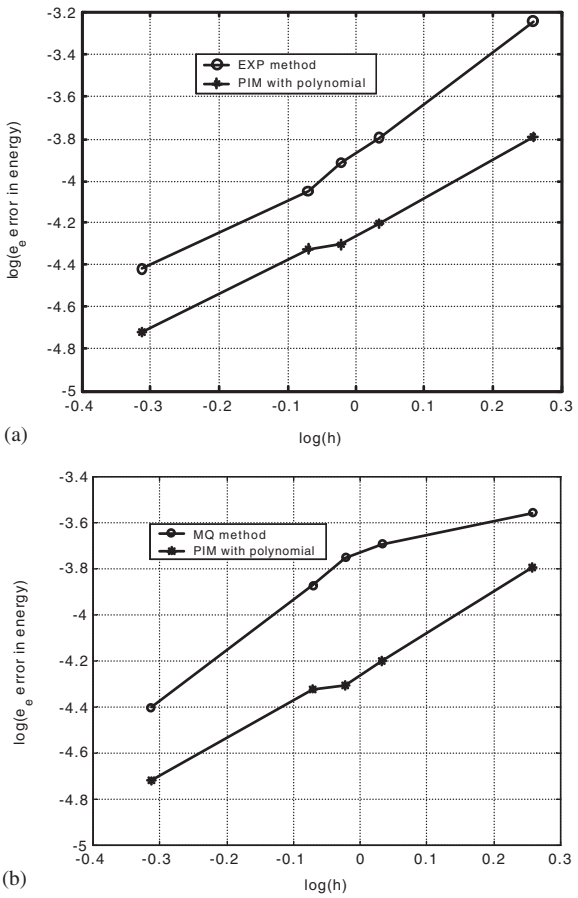

Figure 13. Convergence rate for different basis functions: (a) convergence rate for EXP and polynomial basis; and (b) convergence rate for MQ and polynomial basis.

are imposed on left and bottom edges, and the inner boundary of the hole is traction free. The closed-form solution of stresses is

$$\begin{aligned}
\sigma_x(x,y) &= 1-\frac{a^2}{r^2}\left\{\frac{3}{2}\cos 2\theta+\cos 4\theta\right\}+\frac{3a^4}{2r^4}\cos 4\theta \\
\sigma_y(x,y) &= -\frac{a^2}{r^2}\left\{\frac{1}{2}\cos 2\theta-\cos 4\theta\right\}-\frac{3a^4}{2r^4}\cos 4\theta \\
\sigma_{xy}(x,y) &= -\frac{a^2}{r^2}\left\{\frac{1}{2}\sin 2\theta+\sin 4\theta\right\}+\frac{3a^4}{2r^4}\sin 4\theta
\end{aligned} \tag{38}$$

where (r,θ) are polar co-ordinates and θ is the measured counter-clockwise from the positive x-axis. a is the radius of the hole. For convenience, uniform traction boundary condition is imposed on the right $(x=50)$ edge.

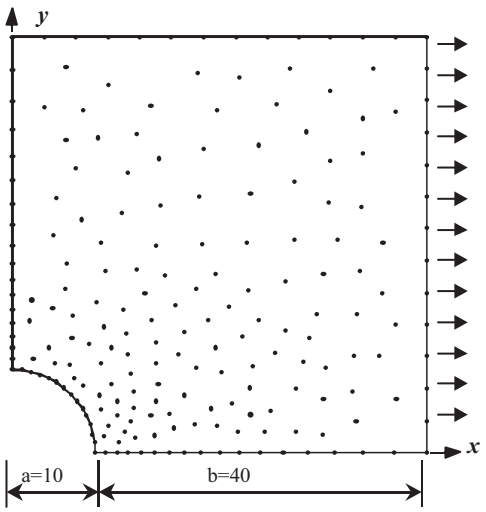

Figure 14. Node distribution in a central-hole plate (subjected to tensile load in the x direction).

6.3.2. Influence domain. Nodes densities for this plate problem vary with positions. The radius $d_{\max}$ of influence domain should be determined for each Gauss point. The neighbouring distance is defined as the square root of weight G_{wt} at that point. Therefore, the $d_{\max}$ is expressed as

$$d_{\max} = D_{\max}\sqrt{G_{\text{wt}}} \tag{39}$$

where G_{wt} is the weight of that Gauss point, which expresses the product of the area included and the Gaussian weight. $D_{\max}$ is an influence coefficient, which is taken as 2.0–6.0 in this example. Nodes are still chosen by a square influence domain. Nodes are limited to maximum 15 and minimum 6. When nodes contained are less than 6, larger $D_{\max}$ is applied. Background cell is composed of triangle cells and quadrature method is used for numerical integration. FEM with constant strain element is also applied to the same problem for comparison. The shape parameter of EXP method is taken to be $c = 0.003$ which is the same as above cantilever beam problem.

6.3.3. Comparison among PIM, FEM and analytical solutions. Figure 15 shows the stress distribution along $y = 10$ section. Results from radial PIM and FEM are almost the same. They are all in good agreement with closed-form solution. Figure 15 also plots the stress distribution at $x = 0$. Closed-form and FEM results are also plotted for comparison. Many authors are accustomed to plotting this figure for comparison [3, 11, 15]. It can be observed from these figures that the EXP method gives satisfactory results. Table III compares the CPU time for radial PIM and FEM for different nodes.

6.4. Tunnel interaction problem

Interaction of two parallel tunnels is studied as an example. The material is assumed to be linearly elastic ($E = 3.0 \times 10^3, v = 0.3$) although real soil/rock is non-linear. Figure 16 shows the node distribution which has total 1270 nodes. Triangle background mesh (2290 cells) is

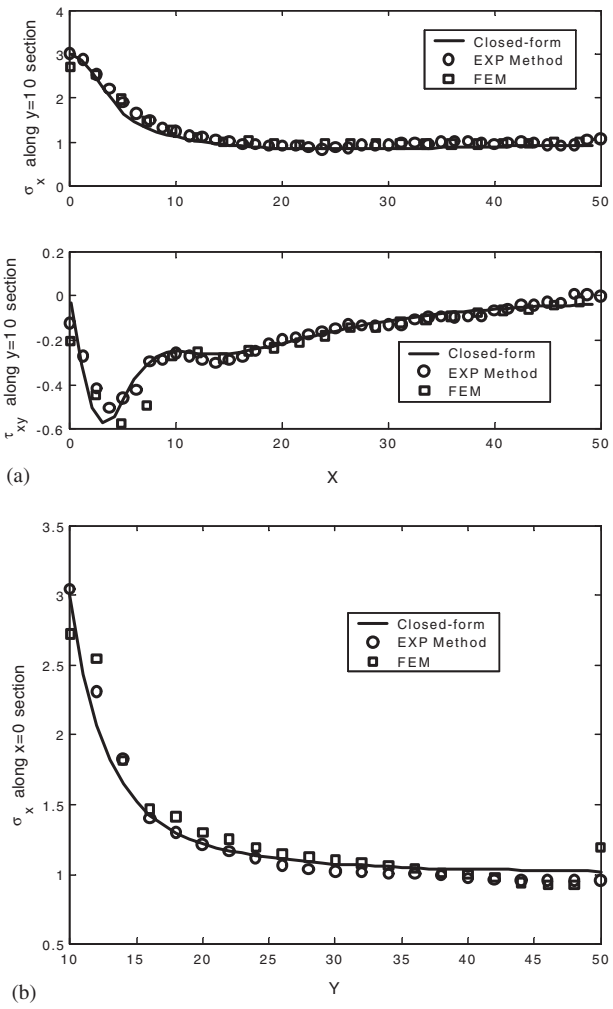

Figure 15. Comparison of EXP method, FEM and closed-form solution: (a) stress distribution along $y = 10$ section; and (b) stress distribution along $x = 10$ section.

Table III. Comparison of CPU time for PIM and FEM.*

Nodes	FEM	Radial PIM
209 (Hole plate)	5 s	5 s
1270 (Tunnel)	2 m 21 s	2 m 46 s

*PIII450 PC is used.

used for numerical integration and one Gauss point is used for each cell. The same background mesh is used for FEM analysis. The soil density is 17 kN/m^3. A strip load (15 kN/m^2) is applied on the top ground between two tunnels. Figure 17 is the typical stress distribution. They are almost the same as FEM results.

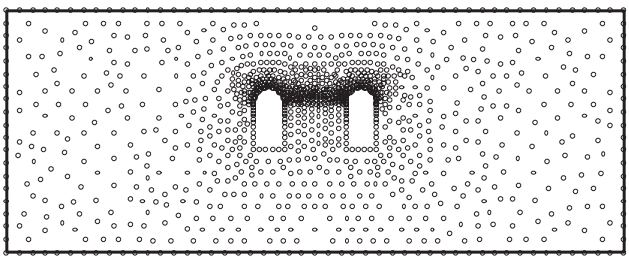

Figure 16. Node distribution for tunnel interaction problem.

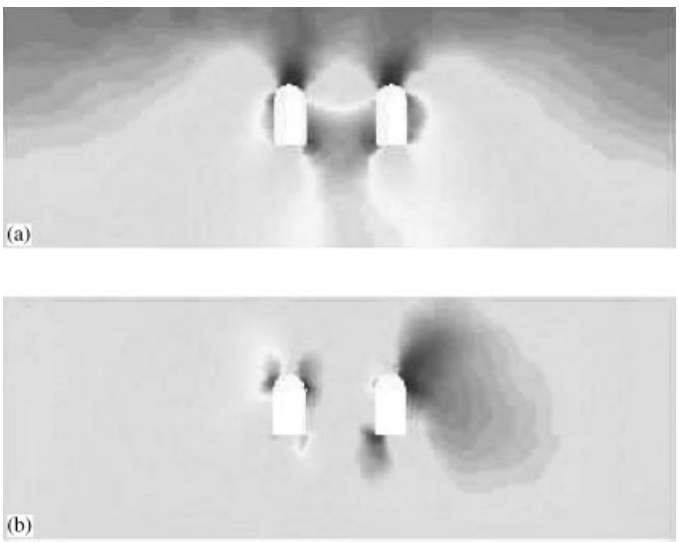

Figure 17. Stress distribution of tunnel interactions (by EXP method): (a) distribution of stress σ_y; and (b) distribution of shear stress τ_{xy}.

7. CONCLUSIONS

A point interpolation meshless method based on radial basis function (radial PIM) is presented and the Gaussian (EXP) and multiquadric (MQ) basis functions are incorporated. First, a general PIM interpolation with the combination of radial and polynomial basis is proposed. Its properties associated with meshless computations are discussed within an influence domain. Then the capability of data fittings for one- and two-dimensional functions is studied under different shape parameters for two particular radial basis functions, MQ and EXP. The interpolation scheme is incorporated with Galerkin weak form of solid mechanics to form the radial PIM. This radial PIM is applied to numerical solutions of partial differential equations. Convergence and accuracy for specified shape parameters are studied through patch test and some example problems in solid mechanics. Through this study, the following conclusions can be made:

(1) The proposed radial PIM has both polynomial and radial basis functions, thus having their advantages. The radial PIM successfully avoids the singularity associated with

the PIM based on only polynomial basis. Including polynomial basis can improve the polynomial accuracy of radial PIM when polynomial functions are approximated. The shape functions obtained are of the property of delta functions, thus overcoming the drawbacks in element-free methods based on MLS approximation. Many computational techniques developed in FEM can be utilized except the concept of elements.

(2) Radial PIM has simple shape functions and derivatives. Once the inverse of matrix **G** is obtained, the shape functions and their derivatives are easily computed with simple multiplication. This computational effort is slightly higher than Jacobean calculation in FEM. Furthermore, the inverse is performed only within an influence domain. The nodes within an influence domain are usually less than 20 in our examples, thus the condition number should not be too high. Radial basis functions are of numerical stability for scattered data points. Our numerical examples show that node points from 6 to 17 can reach sufficient accuracy whether the nodes are structured or unstructured.

(3) Both MQ and EXP interpolations give good accuracy of approximation for function and its derivatives for the three test functions. MQ is of higher accuracy than EXP for one-dimensional function but EXP is better for two-dimensional problems. Both methods have boundary effect for functions and derivatives. Here the boundary effect refers to the derivation of approximation from true values. Further, EXP has smoother approximation for derivative while MQ is smoother in function itself. Therefore, MQ is more suitable for function fitting and EXP is more suitable for the problem that requires derivatives.

(4) Both MQ and EXP methods can reach reasonable precision for cantilever beam problem. MQ method has two shape parameters q and R. If the R is fixed as 1.42, the numerical results are sensitive to the rest shape parameter of q. EXP method has a stable lowest error when its shape parameter is $c=0.002$–0.03. (Not that average number of nodes is about 15.16.) This range of shape parameter is also reasonable for hole plate and tunnel problems. Average number of nodes in an influence domain varying from 6 to 17 can reach good results, although optimum nodes range 10–15. MQ method requires more nodes than EXP method to achieve the same accuracy. Of course, MQ includes two shape parameters and our initial results show that the optimum values of shape parameters are $q=1.03$ and $R=1.42$. These shape parameters are different from the original MQ where $q=0.5$ and reciprocal MQ where $q=-0.5$.

(5) Radial basis functions can be easily extended to multidimensions. This extension just requires slight modification for shape parameters and influence domain. Inclusion of polynomial term can improve the approximation accuracy for simple functions, but the improvement is little for complicated functions. Thus, if fewer nodes are included in an influence domain, polynomial term is recommended. When nodes are 9–16 for a two-dimensional problem, polynomial term is not important.

REFERENCES

1. Nayroles B, Touzot G, Villon P. Generalizing the finite element method: diffuse approximation and diffuse elements. *Computational Mechanics* 1992; **10**:307–318.
2. Lancaster P, Salkauskas K. Surfaces generated by moving least squares methods. *Mathematics of Computation* 1981; **37**:141–158.
3. Belytschko T, Lu Y, Gu L. Element-free Galerkin methods. *International Journal for Numerical Methods in Engineering* 1994; **37**:229–256.

4. Belytschko T, Krongauz Y, Organ D, Fleming M, Krysl P. Meshless methods: an overview and recent developments. *Computational Methods in Applied Mechanics and Engineering* 1996; **139**:3–47.
5. Lu Y, Belytschko T, Gu L. A new implementation of the element-free Galerkin method. *Computational Methods in Applied Mechanics and Engineering* 1994; **113**:397–414.
6. Lucy LB. A numerical approach to the testing of the fission hypothesis. *The Astronomy Journal* 1977; **8**(12):1013–1024.
7. Liu WK, Jun S, Zhang YF. Reproducing kernel particle methods. *International Journal for Numerical Methods in Fluids* 1995; **20**:1081–1106.
8. Duarte CA, Oden JT. Hp clouds—a meshless method to solve boundary-value problems. *Computational Methods in Applied Mechanics and Engineering* 1996; **139**:237–262.
9. Shepard D. A two-dimensional interpolation function for irregularly spaced data. *Proceedings of the ACM National Conference*, 1968; 517–524.
10. Onate E, Idelsohn S, Zienkiewicz OC, Taylor RL. A finite point method in computational mechanic—applications to convective transport and fluid flow. *International Journal for Numerical Methods in Engineering* 1996; **39**:3839–3866.
11. Zhu T, Atluri SN. A modified collocation method and a penalty formulation for enforcing the essential boundary conditions in the element free Galerkin method. *Computational Mechanics* 1998; **21**:211–222.
12. Wagner GJ, Liu WK. Application of essential boundary conditions in mesh-free methods: a corrected collocation method. *International Journal for Numerical Methods in Engineering* 2000; **47**(8):1367–1379.
13. Breitkopf P, Rassineux A, Touzot G, Villon P. Explicit form and efficient computation of MLS shape functions and their derivatives. *International Journal for Numerical Methods in Engineering* 2000; **48**(3):451–466.
14. Danielson KT, Hao S, Liu WK, Aziz Uras R, Li S. Parallel computation of meshless methods for explicit dynamic analysis. *International Journal for Numerical Methods in Engineering* 2000; **47**(7):1323–1341.
15. Liu GR, Gu YT. A point interpolation method for two-dimensional solids. *International Journal for Numerical Methods in Engineering* 2001; **50**:937–951.
16. Liu GR. A point assembly method for stress analysis for solid. In *Impact Response of Materials and Structures*, Shim VPW *et al.* (eds), Oxford University Press, 1999; 475–480.
17. Wang JG, Liu GR, Wu YG. A point interpolation method for simulating dissipation process of consolidation. *Computational Methods in Applied Mechanics and Engineering* 2001; **190**(45):5907–5922.
18. Hardy RL. Theory and applications of the multiquadrics—Biharmonic method (20 years of discovery 1968–1988). *Computers and Mathematics with Applications* 1990; **19**:163–208.
19. Kansa EJ. A scattered data approximation scheme with application to computational fluid-dynamics—I & II. *Computers and Mathematics with Applications* 1990; **19**:127–161.
20. Fasshauer GE. Solving partial differential equations by collocation with radial basis functions. In *Surface Fitting and Multiresolution Methods*, Mehaute AL, Rabut C, Schumaker LL (eds), Nashville, TN: Vanderbilt University Press, 1997; 131–138.
21. Wendland H. Meshless Galerkin method using radial basis functions. *Mathematics of Computation* 1999; **68**(228):1521–1531.
22. Coleman CJ. On the use of radial basis functions in the solution of elliptic boundary value problems. *Computational Mechanics* 1996; **17**:418–422.
23. Wu Z. Compactly supported positive definite radial functions. *Advances in Computational Mathematics* 1995; **4**:283–292.
24. Powell MJD. The theory of radial basis function approximation in 1990. In *Advances in Numerical Analysis*, Light FW (ed.), Oxford: Clarendon Press, 1992; 105–203.
25. Powell MJD. A review of algorithms for thin plate spline interpolation in two dimensions. In *Advanced Topics in Multivariate Approximations*, Fontanella F, Jetter K, Laurent PJ (eds), River Edge, NJ: World Scientific Press, 1996; 303–322.
26. Light W, Wayne H. Error estimates for approximation by radial basis functions. In *Approximation Theory, Wavelets and Applications*, Singh SP (ed.), Dordrecht: Kluwer, 1995; 215–246.
27. Wang JG, Liu GR. On shape parameters for radial PIM meshless method. *Computer Methods in Applied Mechanics and Engineering* 2002; **191**(23–24):2611–2630.
28. Golberg MA, Chen CS, Bowman H. Some recent results and proposals for the use of radial basis functions in the BEM. *Engineering Analysis with Boundary Elements* 1999; **23**:285–296.
29. Franke R. Scattered data interpolation: test of some methods. *Mathematics of Computation* 1982; **38**(157): 181–200.
30. Schaback R. Error estimates and condition numbers for radial basis function interpolation. *Advances in Computational Mathematics* 1995; **3**:251–264.
31. Levesley J. Pointwise estimates for multivariate interpolation using conditionally positive function. Preprint, University of Leicester, 1994.
32. Timoshenko SP, Goodier JN. *Theory of Elasticity* (3rd edn). McGraw-Hill: New York, 1970.

